





Article

Hyaluronic Acid as Macromolecular Crowder in Equine Adipose-Derived Stem Cell Cultures

Sergio Garnica-Galvez ^{1,2,3}, Stefanie H. Korntner ^{3,4} , Ioannis Skoufos ¹, Athina Tzora ¹ , Nikolaos Diakakis ² , Nikitas Prassinou ² and Dimitrios I. Zeugolis ^{3,4,5,6,*} 

- ¹ Laboratory of Animal Science, Nutrition and Biotechnology, Department of Agriculture, University of Ioannina, 47100 Arta, Greece; gsergio@vet.auth.gr (S.G.-G.); jskoufos@uoi.gr (I.S.); tzora@uoi.gr (A.T.)
 - ² School of Veterinary Medicine, Aristotle University of Thessaloniki, 54124 Thessaloniki, Greece; diakakis@vet.auth.gr (N.D.); ngreen@vet.auth.gr (N.P.)
 - ³ Regenerative, Modular & Developmental Engineering Laboratory (REMODEL), Biomedical Sciences Building, National University of Ireland Galway (NUI Galway), H92 W2TY Galway, Ireland; stefanie.korntner@gmail.com
 - ⁴ Science Foundation Ireland (SFI) Centre for Research in Medical Devices (CÚRAM), Biomedical Sciences Building, National University of Ireland Galway (NUI Galway), H92 W2TY Galway, Ireland
 - ⁵ Regenerative, Modular & Developmental Engineering Laboratory (REMODEL), Faculty of Biomedical Sciences, Università della Svizzera Italiana (USI), 6904 Lugano, Switzerland
 - ⁶ Regenerative, Modular & Developmental Engineering Laboratory (REMODEL), School of Mechanical and Materials Engineering, University College Dublin (UCD), D04 V1W8 Dublin, Ireland
- * Correspondence: dimitrios.zeugolis@ucd.ie



Citation: Garnica-Galvez, S.; Korntner, S.H.; Skoufos, I.; Tzora, A.; Diakakis, N.; Prassinou, N.; Zeugolis, D.I. Hyaluronic Acid as Macromolecular Crowder in Equine Adipose-Derived Stem Cell Cultures. *Cells* **2021**, *10*, 859. <https://doi.org/10.3390/cells10040859>

Academic Editor: Friedrich Jung

Received: 6 March 2021

Accepted: 7 April 2021

Published: 9 April 2021

Publisher's Note: MDPI stays neutral with regard to jurisdictional claims in published maps and institutional affiliations.



Copyright: © 2021 by the authors. Licensee MDPI, Basel, Switzerland. This article is an open access article distributed under the terms and conditions of the Creative Commons Attribution (CC BY) license (<https://creativecommons.org/licenses/by/4.0/>).

Abstract: The use of macromolecular crowding in the development of extracellular matrix-rich cell-assembled tissue equivalents is continuously gaining pace in regenerative engineering. Despite the significant advancements in the field, the optimal macromolecular crowder still remains elusive. Herein, the physicochemical properties of different concentrations of different molecular weights hyaluronic acid (HA) and their influence on equine adipose-derived stem cell cultures were assessed. Within the different concentrations and molecular weight HAs, the 10 mg/mL 100 kDa and 500 kDa HAs exhibited the highest negative charge and hydrodynamic radius, and the 10 mg/mL 100 kDa HA exhibited the lowest polydispersity index and the highest % fraction volume occupancy. Although HA had the potential to act as a macromolecular crowding agent, it did not outperform carrageenan and Ficoll[®], the most widely used macromolecular crowding molecules, in enhanced and accelerated collagen I, collagen III and collagen IV deposition.

Keywords: excluded volume effect; extracellular matrix deposition; organogenesis

1. Introduction

Cell-assembled tissue engineering has the potential to revolutionise reparative biomedicine, as it takes advantage of the cells' natural intrinsic abilities to fabricate tissues with complexity, precision and efficiency that human-made devices have yet to reach. Despite the repeatedly demonstrated safety and efficacy in the clinical setting (e.g., cardiac [1], cartilage [2], cornea [3] and skin [4]), only a handful of concepts have passed the 'valley of death' to become commercial reality. It is accepted that the major culprit in the development of cell-based scaffold-free tissue engineering products is the lengthy period of time *ex vivo* (up to 196 days for blood vessels [5]) that is associated with losses in cell function [6] and extremely high manufacturing costs [7]. To this end, strategies that enhance and accelerate extracellular matrix (ECM) synthesis and deposition, whilst controlling cell fate during *in vitro* expansion should be incorporated into the developmental cycle of advanced therapy medicinal products to develop clinically and commercially relevant products.

It has been well-documented that among the various *in vitro* microenvironment modulators (e.g., surface topography [8], substrate rigidity [9], oxygen tension [10], me-

chanical stimulation [11] and growth factor supplementation [12]), macromolecular crowding (MMC) is the only one that profoundly enhances (up to 120-fold) and accelerates (within 6 days in culture) ECM deposition, due to its negative charge and high polydispersity [13–15]. This unprecedented success of MMC in eukaryotic cell culture lays on the fact that in traditionally used dilute cell culture systems, the enzymatic conversion of water-soluble procollagen to water-insoluble collagen is very slow [16], as the proteinases and the procollagen are diffused in the culture media, whilst in crowded cell culture systems, this enzymatic processing of collagen is rapid, as the proteinases and the procollagen are confined at the interface of cell-layer/crowders [17]. The effectiveness of MMC is based on its mechanism of action; due to steric hindrance and/or electrostatic repulsion, macromolecules in highly volume-occupied or crowded solutions exclude each other from their respective vicinity, as two macromolecules cannot occupy the same space at the same time (excluded volume effect) [18]. This excluded volume effect decreases diffusion in a system, via the obstruction of molecular motion [19], which unavoidably affects the thermodynamics, kinetics and equilibria of biochemical reactions and biological processes (e.g., DNA structure, stability, condensation and replication [20–22]; RNA and protein transcription, structure and folding [23–25]), subject to the physicochemical properties (e.g., charge [26], dispersity [27], size [28], shape [29] and viscosity [30]) of the MMC agents.

In cell culture, several macromolecules have been assessed as MMC agents over the years, largely categorised as non-sulphated polysaccharides (e.g., Ficoll® [31]), sulphated polysaccharides (e.g., carrageenan [15]) and polymers (e.g., polyvinylpyrrolidone [32]). Although carrageenan, due to its negative charge and polydispersity, has been shown to induce the highest ECM deposition (up to a 120-fold increase) in the shortest period of time (within 6 days) [13], its questionable association with colitis [33–35] imposes the need to identify alternative molecules. In the quest for the ideal MMC agent, hyaluronic acid (HA) was recently utilised in human neonatal fibroblast cultures [36]. Although this proof of principle study demonstrated the potential of 1500 kDa HA to act as an MMC agent, the optimal HA molecular weight and concentration were not identified and the physicochemical properties (e.g., charge, hydrodynamic radius, polydispersity) were not assessed, which are of significant importance, considering that the effectiveness of HA as an MMC/volume exclusion agent lays on its capacity to bind and retain water molecules (up to 6 L per g) [37,38] in a size-, shape-, concentration- and viscosity-dependent manner [39]. Herein, we ventured to comprehensively assess the physicochemical properties of different concentrations of different molecular weight HAs in equine adipose-derived stem cell (eADSC) cultures.

2. Materials and Methods

2.1. Materials

Cell culture plasticware and chemicals/reagents were purchased from Sarstedt (Nümbrecht, Germany) and Sigma-Aldrich (Athens, Greece), respectively, unless otherwise stated (catalogue numbers are mentioned in brackets). HAs of different molecular weight (10 (10 to 20 kDa), 60 (66 to 99 kDa), 100 (100 to 150 kDa), 500 (301 to 450 kDa) and 1000 kDa (750 to 1000 kDa)) were purchased from Lifecore™ Biomedical (Chaska, MN, USA). Equine fat tissues, from the mane, were provided from the School of Veterinary Medicine, Aristotle University of Thessaloniki, Thessaloniki, Greece.

2.2. Stem Cell Extraction, Expansion, Cryopreservation and Thawing

Fat samples were washed with Hanks' Balanced Salt Solution (HBSS, XC-S2064, Biosera, Nuaille, France) containing 1% penicillin/streptomycin (P/S, P4333), minced with sterile dissection material and enzymatically digested with 0.1% collagenase from *Clostridium histolyticum* (C9722). Collagenase digestion was performed for 4 h at 37 °C in standard cell culture media (Dulbecco's Modified Eagle Medium high glucose (DMEM, D6429), 10% foetal bovine serum (FBS, F7524) and 1% P/S). Fat tissue stromal vascular fraction (SVF) was obtained by centrifugation of digested samples for 5 min at 700 g (4 times). SVF

was resuspended in standard cell culture media and passed through a Corning® nylon cell strainer of 70 µm (CLS431751). Nucleated cells from the SVF were counted using a Neubauer chamber and seeded at a density of 2,000,000 cells/cm² in tissue culture flasks at 37 °C in a humidified atmosphere of 5% CO₂. Media were changed every 3–4 days (the cells were washed twice with 1% P/S in phosphate buffered saline, PBS, to remove non-attached cells before fresh media were added) until the cells reached ~ 80% confluency. Cell detachment was carried out using trypsin-ethylenediaminetetraacetic acid (EDTA) solution (T3924) for 5 min at 37 °C in a humidified atmosphere of 5% CO₂. Cell suspensions were centrifuged for 5 min at 700 g and then seeded at a density of 5000 cells/cm² in standard cell culture media (DMEM, 10% FBS, 1% P/S) and conditions (37 °C, humidified atmosphere of 5% CO₂). At passage 2–3, cell culture flasks were tested for mycoplasma [40]. Mycoplasma-free cells were stored in liquid nitrogen in 1.6 mL CryoPure tubes, each containing 1.8–2.0 × 10⁶ cells in 1 mL 90% FBS /10% dimethyl sulfoxide (DMSO). The cryovials were frozen at –80 °C in a Nalgene® Mr. Frosty freezing container (C1562) and transferred to the liquid nitrogen storage after 24 h. Prior to use, cryovials were thawed in a thermostatic bath at 37 °C and cells were seeded in pre-equilibrated tissue culture flasks in standard cell culture media and conditions at 5000 cells/cm². After 24 h, the media were changed to ensure complete removal of DMSO. From then onwards, the media were changed every 3–4 days until reaching 80% confluency and passage 4. All experiments were conducted with cells at passage 5.

2.3. Cell Morphology Analysis

Cell morphology was assessed via bright field microscopy using an inverted Olympus IX73 microscope (Olympus Corporation, Tokyo, Japan).

2.4. Stem Cell Characterisation Analysis

Multipotency was assessed with established osteogenic, adipogenic and chondrogenic protocols, using cells in DMEM as negative controls, and surface markers were assessed with fluorescence-activated cell sorting (FACS) analysis, validating the antibodies with immunocytochemistry.

2.4.1. Osteogenic Analysis

For osteogenesis, 5000 cells/cm² were seeded in 6-well plates. Standard cell culture media was substituted after 24 h by osteo-induction media consisting of 100 nM dexamethasone (D4902), 100 µM L-ascorbic acid 2-phosphate (A8960) and 10 mM β-glycerophosphate disodium salt hydrate (G9422) in 10% FBS and 1% P/S. Osteo-induction media were changed every 3 days up to day 14. At day 14, cell layers were treated with methanol at 4 °C for 20 min and calcium depots were detected by adding 400 µL of 40 mM alizarin red S stain (A5533), pH 4.1. Excess dye was removed with PBS washes.

2.4.2. Adipogenic Analysis

For adipogenesis, 2500 cells/cm² were seeded in 6-well plates. After 3 days the media were changed to adipo-induction media consisting of 0.1 µM dexamethasone, 500 µM 3-isobutyl-1-methylxanthine (IBMX, I5879), 200 µM indomethacin (I7378), 15% horse serum (H1270) and 1% P/S. The adipo-induction media was changed every 3 days up to day 18. At day 18, cell layers were treated with 10% formalin for 15 min at room temperature and lipid droplets were detected by adding 400 µL of 0.3% red oil O stain (O1391) in 60% isopropanol. Excess dye was removed with PBS washes.

2.4.3. Chondrogenic Analysis

For chondrogenesis, pellet cultures were performed. Approximately 500,000 cells were pelleted into 15 mL conical polypropylene tubes with chondro-induction media consisting of serum-free DMEM High Glucose, 100 nM dexamethasone, 100× ITS + 1 (Insulin-transferrin-sodium selenite, linoleic-bovine serum albumin, BSA) liquid media

supplement (I2521; 1× dilution in the final chondro-induction media), 40 µg/mL L-proline (P5607), 25 µg/mL L-ascorbic acid 2-phosphate, 10 ng/mL TGF-β3 (R&D Systems, UK, 8420-B3/CF) and 1% P/S. The chondro-induction media were changed every 3 days up to day 21. At day 21, pellets were cryoprotected with increasing gradient (15 and 30%) sucrose solutions. Cryoprotected pellets were embedded in optimal cutting temperature compound and frozen in liquid nitrogen. Sections 5 µm thick were obtained using a Leica CM1850 (Leica Microsystems, Milton Keynes, UK) cryotome. Sections were stained with Alcian blue (B8438), washed with 1% acetic acid, stained with nuclear fast red aluminium solution 0.1% (100121), washed with double-distilled water, dehydrated in 100% ethanol and mounted using DPX mountant for histology (06522). Images of osteogenic and adipogenic induction were captured with an Olympus IX73 microscope (Olympus Corporation, Tokyo, Japan) and images of chondrogenic induction were captured with an Olympus BX51 microscope (Olympus Corporation, Tokyo, Japan).

2.4.4. FACS Analysis

A FACScalibur™ (BD, Wokingham, UK) device was used for cell surface markers analysis. Briefly, at 80% confluency at passage 5, cells were trypsinised and suspended at 2×10^6 cells/mL density in 2 mM EDTA/PBS buffer. 50 µL aliquots were tested in flow cytometry tubes and incubated for 30 min at 4 °C with the following antibodies: AlexaFluor® 488 anti-human CD29 (BioLegend®, San Diego, CA, USA, clone TS2/16) [41,42], FITC mouse anti-human CD34 (BD Pharmingen™, Wokingham, UK, clone 581) [43–45], FITC mouse anti-horse CD44 (Bio-Rad Laboratories, Watford, Hertfordshire, UK, clone CV58) [43–45], PE mouse anti-human CD90 (BD Pharmingen™, Wokingham, UK, clone 5E10) [41,42,46] and PE mouse anti-human CD105 (ThermoFisher Scientific, Gloucester, UK, clone SN6) [44]. PE- and FITC-conjugated mouse IgG1, κ isotype controls (BD Pharmingen™, Wokingham, UK, clone MOPC21), were used to discard unspecific binding and cells alone as negative controls to eliminate autofluorescence. SYTOX™ Red Dead Cell Stain (ThermoFisher Scientific, Gloucester, UK, S3459) at a final concentration of 1 µM was used to distinguish viable and non-viable cells. Analysis was performed by using BD CellQuest™ software (BD, Wokingham, UK).

To validate the antibodies used for FACS analysis, immunocytochemistry was also carried out when the cells reached 80% confluency. Secondary antibodies were not used, as the CD markers used for FACS analysis were directly conjugated to the aforementioned fluorochromes. The antibodies were incubated at 4 °C overnight. Details of the immunocytochemistry analysis are provided below.

2.5. Solubility Analysis

In order to identify working concentrations of the different molecular weight (10, 60, 100, 500 and 1000 kDa) HAs, different concentrations (0.1, 0.5, 1, 5, 10, 20, 30, 50, 60, 100, 200 and 500 mg/mL) of each HA molecular weight were dissolved in standard cell culture media at 37 °C. Optimal concentrations from this experiment were also screened with cells in standard cell culture media under standard cell culture conditions after 4 days in culture (see below).

2.6. Dynamic Light Scattering Analysis

Zeta potential, polydispersity index and hydrodynamic radius were assessed using dynamic light scattering (Zetasizer ZS90, Malvern Instruments, Malvern, UK). The crowding solutions were prepared in PBS to mimic physiological conditions. Fractional volume occupancy was calculated using the obtained values of hydrodynamic radius for the different MMC agents, as has been described before [47].

2.7. Stem Cell Culture

Cells were seeded at a 15,000 cells/cm² density in standard cell culture media supplemented with 100 µM L-ascorbic acid 2-phosphate to induce collagen synthesis. After

24 h, media were changed and replaced with media containing the different concentrations of the different HA molecular weights. Media without MMC and media with carrageenan (75 µg/mL, C1013) and Ficoll® (cocktail of 37.5 mg/mL Ficoll® 70 kDa, F2878 and 25 mg/mL Ficoll® 400 kDa, F4375) were used as controls. All crowders were sterilised under UV light for 15 min and solubilised in standard cell culture media supplemented with L-ascorbic acid 2-phosphate at 37 °C until no particles in suspension were observed. Media changes were performed every 2 days until reaching day 8. The workflow is schematically illustrated in Supplementary Figure S1.

2.8. Stem Cell Viability Analysis

A Live/Dead® viability kit (L3224, Invitrogen™, Gloucester, UK) was used to assess cell viability, as per manufacturer's protocol. Briefly, at each timepoint, cells were washed with HBSS and incubated with a solution containing 2 µM calcein-AM and 4 µM ethidium homodimer in HBSS for 30 min at 37 °C in a 5% CO₂ humidified atmosphere. DMSO was added for positive dead cell controls. Excess dye was removed by washing with HBSS. Samples were visualised using an inverted IX73 Olympus microscope (Olympus Corporation, Tokyo, Japan). At least 5 regions of interest (ROI) per image were selected. Alive and dead cells were counted with ImageJ software (NIH, Bethesda, MD, USA) and percentage cell viability was calculated as alive cell number against total cell number.

2.9. Stem Cell Proliferation Analysis

Cell proliferation was assessed via nuclei counting. Briefly, cell cultures were washed with HBSS at each timepoint and fixed with a filtered (0.2 µm sterile syringe filter) solution of 2% paraformaldehyde (PFA) in PBS. Excess fixation solution was removed by PBS washes. Samples were then incubated for 5 min in a 4',6-diamidino-2-phenylindole (DAPI, D1306, Invitrogen™, Gloucester, UK) in methanol at 0.5 µg/mL concentration solution. Excess DAPI solution was removed with PBS washes. Samples were visualised using an inverted IX73 Olympus microscope (Olympus Corporation, Tokyo, Japan). Cell nuclei were counted with ImageJ software (NIH, Bethesda, MD, USA); the watershed plugin was used to separate overlapped nuclei. At least 5 ROI per image were selected. Nuclei were counted to obtain cell number per area at the different timepoints.

2.10. Stem Cell Metabolic Activity Analysis

Cell metabolic activity was assessed using the alamarBlue™ (DAL1025, Invitrogen™, Gloucester, UK) assay, as per manufacturer's protocol. Briefly, at the end of each culture timepoint, cells were washed with HBSS and 10% alamarBlue™ solution in HBSS was added. Samples were incubated for 3 h at 37 °C in a 5% CO₂ humidified atmosphere. Absorbance at 550 nm excitation and 595 nm emission was then measured using a plate reader (ELx800, Biotek, Swindon, UK). Cell metabolic activity was expressed as the% reduction in the alamarBlue® dye and normalised to the control group without MMC.

2.11. Gel Electrophoresis Analysis

At each timepoint collagen extraction from the cell layers and sodium dodecyl sulphate-polyacrylamide gel electrophoresis (SDS-PAGE) was performed [48]. Briefly, at each timepoint, cell culture media were removed and the cell layers were washed twice with HBSS at 37 °C. Cell layers were digested with pepsin from porcine gastric mucosa (P6887; 150 µL per well of a 24-well plate at a final concentration of 0.1 mg/mL in 0.05 M acetic acid) for 2 h at 37 °C under continuous shaking. Then, 100 µL of the digested cell layers were collected and neutralised with 20 µL of 0.1 N NaOH. Samples were either analysed immediately or stored at −80 °C until analysis. Digested and neutralised samples were appropriately diluted with distilled water and 5× sample buffer and heated at 95 °C for 5 min. Per well, 15 µL per sample solution was loaded on the gel (3% stacking gel/5% running gel). As a reference standard, 15 µL of 0.1 mg/mL in 0.05 M acetic acid bovine skin collagen type I (CBPE2US010, Symatase Biomateriaux, Chaponost, France) was

used. Electrophoresis was performed in a Mini-PROTEAN Tetra Electrophoresis System (Bio-Rad, Watford, Hertfordshire, UK) by applying a potential difference of 50 mV for the initial 30–40 min and then 110 mV for the remaining time (50–70 min). The gels were washed with double-distilled water and stained using the PlusOne™ Silver Staining Kit, Protein (17115001, GE Healthcare, Chalfont St Giles, Buckinghamshire, UK), according to the manufacturer's protocol. Images of the gels were taken after brief washing with double-distilled water. To quantify the cell-produced collagen type I deposition, the relative densities of collagen α 1(I) and α 2(I) chains were evaluated using ImageJ software (NIH, Bethesda, MD, USA) after applying the background subtraction plugin and correlated to the α 1(I) and α 2(I) chain bands densities of the reference standard collagen type I.

2.12. Immunocytochemistry Analysis

At each timepoint, media were removed, samples were washed with HBSS and fixed for 15 min with filtered 2% PFA at 4 °C. Excess PFA was removed with PBS washes. Blocking of non-specific bindings was performed with a 3% BSA (A7638) solution at room temperature for 30 min. The samples were then incubated for 90 min at room temperature with the following primary antibodies: mouse monoclonal anti-collagen type I (ab90395, 1:500 dilution), rabbit polyclonal anti-collagen type III (ab7778, 1:200 dilution) and rabbit polyclonal anti-collagen type IV (ab6586, 1:200 dilution); all Abcam, Ireland. The samples were washed 3 times with PBS and then incubated for 30 min with the following secondary antibodies at 1:500 dilution: goat anti-rabbit conjugated to AlexaFluor® 488 (A-32731) and goat anti-mouse conjugated AlexaFluor® 555 (A-32727); both ThermoFisher Scientific (Dublin, Ireland). As negative controls to subtract the background, the samples were incubated in PBS without primary antibodies and incubated with the corresponding secondary antibodies. Samples were washed 3 times with PBS and incubated for 5 min with DAPI at 0.5 μ g/mL concentration in methanol. The samples were washed 3 times with PBS and mounted with 10 μ L of VECTASHIELD® HardSet™ Antifade Mounting Medium (H1500, Vector Laboratories, Burlingame, CA, USA). Glass coverslips with a diameter of 8 mm were placed on top of the samples. Images were taken with an Olympus IX73 inverted microscope (Olympus Corporation, Japan). The Q-Capture Pro 7 software (QImaging, Rockville, Maryland, USA) was used for image acquisition. At least 5 ROI per image were selected. Fluorescence intensity was calculated using the ImageJ software (NIH, Bethesda, MD, USA), subtracting from every ROI the average fluorescence intensity value of the negative control. The values were normalised to the corresponding cell number of each ROI.

2.13. Statistical Analysis

Numerical data are expressed as mean \pm standard deviation (SD). Data were processed in Microsoft® Excel and statistical analysis was performed using SigmaPlot® 12.0 software (Systat Software, Slough, UK). One way analysis of variance (ANOVA) followed by pairwise multiple comparison (Holm-Sidak's method) was used when the distributions of the populations were normal (Shapiro-Wilk normality test) and the variances of populations were equal (Levene's test). Non-parametric analysis was performed using Kruskal-Wallis followed by Dunn's multiple comparison post-hoc analysis for pairwise multiple comparisons, when the assumptions of parametric analysis were violated. Statistical significance was accepted at $p < 0.05$.

3. Results

3.1. Stem Cell Characterisation

The extracted cells were mesenchymal in origin as trilineage analysis (Figure S2A) revealed calcium deposits in osteogenic media, lipid droplets in adipogenic media and glycosaminoglycan-rich ECM in chondrogenic media; FACS analysis (Figure S2B) demonstrated that the cells were positive for CD90 (95.2% \pm 0.3%), CD44 (58.4% \pm 1.4%) and

CD29 (41.7% ± 11.5%) and negative for CD105 (0.1% ± 0.0%) and CD34 (0.0% ± 0.0%); and immunocytochemistry analysis (Figure S2C) visually corroborated the FACS analysis data.

3.2. HA Solubility Assessment

Solubility assessment in cell-free standard cell culture media at 37 °C (Table S1) revealed that the 10 kDa HA was soluble up to 200 mg/mL; the 60 kDa HA was soluble up to 60 mg/mL; the 100 kDa HA was soluble up to 30 mg/mL; the 500 kDa HA was soluble up to 10 mg/mL; and the 1000 kDa HA was soluble up to 5 mg/mL. Subsequent bright field microscopy analysis after 4 days in culture (Figure S3) revealed that all concentrations of the 10 kDa HA, the 30 and 60 mg/mL concentrations of the 60 kDa HA and the 30 mg/mL concentration of the 100 kDa HA resulted in cell detachment, and the 20 mg/mL concentration of the 100 kDa HA resulted in microgel formation; thus, they were discarded for further analysis.

3.3. Dynamic Light Scattering Assessment

Zeta potential analysis (Table 1) revealed that all HA 60 kDa, HA 100 kDa (but the 10 mg/mL), HA 500 kDa (but the 10 mg/mL) and HA 1000 kDa concentrations exhibited a significantly ($p < 0.05$) lower negative charge than carrageenan; and that carrageenan and all HA 60 kDa, HA 100 kDa (but the 0.5 mg/mL), HA 500 kDa (but the 0.5 mg/mL) and HA 1000 kDa concentrations exhibited a significantly ($p < 0.05$) higher negative charge than Ficoll®. Within the different HA molecular weights, for HA 60 kDa and HA 1000 kDa, the charge was not affected ($p > 0.05$) as a function of increased concentration, whilst for HA 100 kDa and HA 500 kDa, the charge was significantly ($p < 0.05$) decreased as a function of increased concentration (Table 1).

Table 1. Dynamic light scattering analysis.

Polymer (Concentration)	Zeta Potential (mV)	Hydrodynamic Radius (nm)	Polydispersity Index	Fractional Volume Occupancy (%)
FC 70 (25 mg/mL) + FC 400 (37.5 mg/mL)	-2.2 ± 1.1 #	15 ± 1 #	0.77 ± 0.11	(111 ± 13)
CR (75 µg/mL)	-26.5 ± 6.7 *	140 ± 29	0.68 ± 0.11	(1019 ± 570)
HA 60 (0.5 mg/mL)	-11.8 ± 1.9	246 ± 68	0.88 ± 0.12	(36,140 ± 29,701)
HA 60 (1 mg/mL)	-10.8 ± 1.6	302 ± 60	0.89 ± 0.12	(124,894 ± 61,980)
HA 60 (5 mg/mL)	-13.3 ± 0.8	249 ± 133	0.87 ± 0.11	(516,151 ± 631,032)
HA 60 (10 mg/mL)	-13.1 ± 2.7	262 ± 108	0.86 ± 0.12	(995,364 ± 771,048 +)
HA 100 (0.5 mg/mL)	-2.6 ± 2.3 #	85 ± 10	0.51 ± 0.06	(784 ± 264)
HA 100 (1 mg/mL)	-12.8 ± 1.6	194 ± 113	0.68 ± 0.37	(5448 ± 116)
HA 100 (5 mg/mL)	-16.0 ± 4.9	570 ± 17	0.60 ± 0.11	(2,341,046 ± 211,149)
HA 100 (10 mg/mL)	-23.2 ± 2.1 *, +	1886 ± 123 *, +	0.35 ± 0.02 #	(170,651,055 ± 33,934,948 *, +)
HA 500 (0.5 mg/mL)	-3.7 ± 0.7 #	59 ± 15	0.86 ± 0.12	59 ± 37
HA 500 (1 mg/mL)	-8.8 ± 2.6	46 ± 8	0.92 ± 0.08	51 ± 26
HA 500 (5 mg/mL)	-18.0 ± 3.1	213 ± 36	1.00 ± 0.00	(25,933 ± 12,345)
HA 500 (10 mg/mL)	-25.8 ± 3.3 *, +	604 ± 68 +	1.00 ± 0.00	(1,140,733 ± 384,037 +)
HA 1000 (0.1 mg/mL)	-7.1 ± 4.0	70 ± 24	0.97 ± 0.03	11 ± 8 #
HA 1000 (0.5 mg/mL)	-6.9 ± 4.2	99 ± 53	0.96 ± 0.08	(193 ± 226)
HA 1000 (1 mg/mL)	-9.0 ± 2.5	95 ± 29	0.78 ± 0.18	(256 ± 204)
HA 1000 (5 mg/mL)	-12.4 ± 1.5	133 ± 40	0.64 ± 0.09	(3484 ± 2294 +)

All molecules were negatively charged and, among all molecules and concentrations, the FC and the 0.5 mg/mL HA 60 kDa and HA 100 kDa exhibited the highest ($p < 0.05$) charge. The 10 mg/mL HA 100 kDa and the Ficoll® exhibited the highest ($p < 0.05$) and the lowest ($p < 0.05$) hydrodynamic radius, respectively. The 10 mg/mL HA 100 kDa exhibited the lowest ($p < 0.05$) polydispersity index. The 10 mg/mL HA 100 kDa and the 0.1 mg/mL HA 1000 kDa exhibited the highest ($p < 0.05$) and the lowest ($p < 0.05$) % fraction volume occupancy, respectively. * indicates significantly ($p < 0.05$) higher values among all groups. + indicates significantly ($p < 0.05$) higher values within a given HA molecular weight. # indicates significantly ($p < 0.05$) lower values among all groups. In parentheses, the calculated % fractional volume occupancy values, but as the values are > 100%, they cannot be considered as pragmatic. FC: Ficoll®. CR: Carrageenan. HA: Hyaluronic acid

Hydrodynamic radius analysis (Table 1) revealed that all concentrations of HA 60 kDa, the 5 and 10 mg/mL concentrations of HA 100 kDa and the 5 and 10 mg/mL concentrations of HA 500 kDa exhibited a significantly ($p < 0.05$) higher hydrodynamic radius than carrageenan; that the 0.5 mg/mL concentration of HA 100 kDa, the 0.5 and 1 mg/mL concentrations of HA 500 kDa and the 0.1 mg/mL concentration of HA 1000 kDa exhibited a significantly ($p < 0.05$) lower hydrodynamic radius than carrageenan; and that carrageenan and all concentrations of HA 60 kDa, HA 100 kDa, HA 500 kDa and HA 1000 kDa exhibited a significantly ($p < 0.05$) higher hydrodynamic radius than Ficoll®. Within the different HA molecular weights, for HA 60 kDa and HA 1000 kDa, the hydrodynamic radius was not affected ($p > 0.05$) as a function of increased concentration, whilst for HA 100 kDa and HA 500 kDa, the hydrodynamic radius was not significantly ($p > 0.05$) affected between 0.5 and 1 mg/mL concentration and was significantly ($p < 0.05$) increased as a function of increased (from 1 to 5 mg/mL and from 5 to 10 mg/mL) concentration (Table 1).

Polydispersity analysis (Table 1) revealed no significant differences in polydispersity between carrageenan, Ficoll® and all concentrations of HA 60 kDa, HA 100 kDa (apart from the 10 mg/mL concentration which was the lowest ($p < 0.05$) of all), HA 500 kDa and HA 1000 kDa.

Fractional volume occupancy (%) analysis (Table 1) revealed that carrageenan exhibited a significantly ($p < 0.05$) higher % fractional volume occupancy than Ficoll® and all HA 60 kDa concentrations, the 1, 5 and 10 mg/mL HA 100 kDa concentrations, the 5 and 10 mg/mL HA 500 kDa concentrations and the 5 mg/mL HA 1000 kDa concentration exhibited a significantly ($p < 0.05$) higher % fractional volume occupancy than carrageenan and Ficoll®. Within the different HA molecular weights, the highest concentration of HA 60 kDa (10 mg/mL), HA 100 kDa (10 mg/mL), HA 500 kDa (10 mg/mL) and HA 1000 kDa (5 mg/mL) exhibited the highest ($p < 0.05$) % fractional volume occupancy (Table 1). Among all groups, the 10 mg/mL HA 100 kDa and the 0.1 mg/mL HA 1000 kDa exhibited the highest ($p < 0.05$) and the lowest ($p < 0.05$) % fractional volume occupancy, respectively (Table 1).

3.4. Cell Morphology Assessment

Bright field microscopy analysis (Figure S4) revealed no apparent differences at any timepoint in cell morphology as a function of MMC, independently of the MMC agent used and its respective concentration.

3.5. Cell Viability, Proliferation and Metabolic Activity Assessment

Qualitative (Figure S5) and quantitative (Figure S6A) cell viability analysis revealed no apparent differences at any timepoint in cell viability as a function of MMC, independently of the MMC agent used and its respective concentration.

Quantitative cell proliferation (Figure S6B) and metabolic activity (Figure S6C) analyses revealed that the Ficoll® at all timepoints and the carrageenan, the 10 mg/mL HA 100 kDa, the 5 and 10 mg/mL HA 500 kDa and the 5 mg/mL HA 1000 kDa at day 8 significantly ($p < 0.05$) decreased cell number and increased cell metabolic activity.

3.6. Gel Electrophoresis Assessment

SDS-PAGE and complementary densitometry analyses (Figure 1) revealed that carrageenan induced the highest ($p < 0.05$) collagen type I deposition at all timepoints and Ficoll® induced significantly ($p < 0.05$) higher collagen type I deposition than the non-MMC group only at day 4 and in some instances, at day 8, induced the lowest ($p < 0.05$) collagen type I deposition. The high concentrations (5 and 10 mg/mL) of HA 60 kDa (Figure 1) and HA 100 kDa (Figure 1) induced significantly ($p < 0.05$) higher collagen type I deposition than the non-MMC group only at day 4. The 5 mg/mL concentration of HA 500 kDa (Figure 1) induced significantly ($p < 0.05$) higher collagen type I deposition than the non-MMC group only at day 4. None of the HA 1000 kDa (Figure 1) concentrations

induced significantly ($p > 0.05$) higher collagen type I deposition than the non-MMC group at any timepoint.

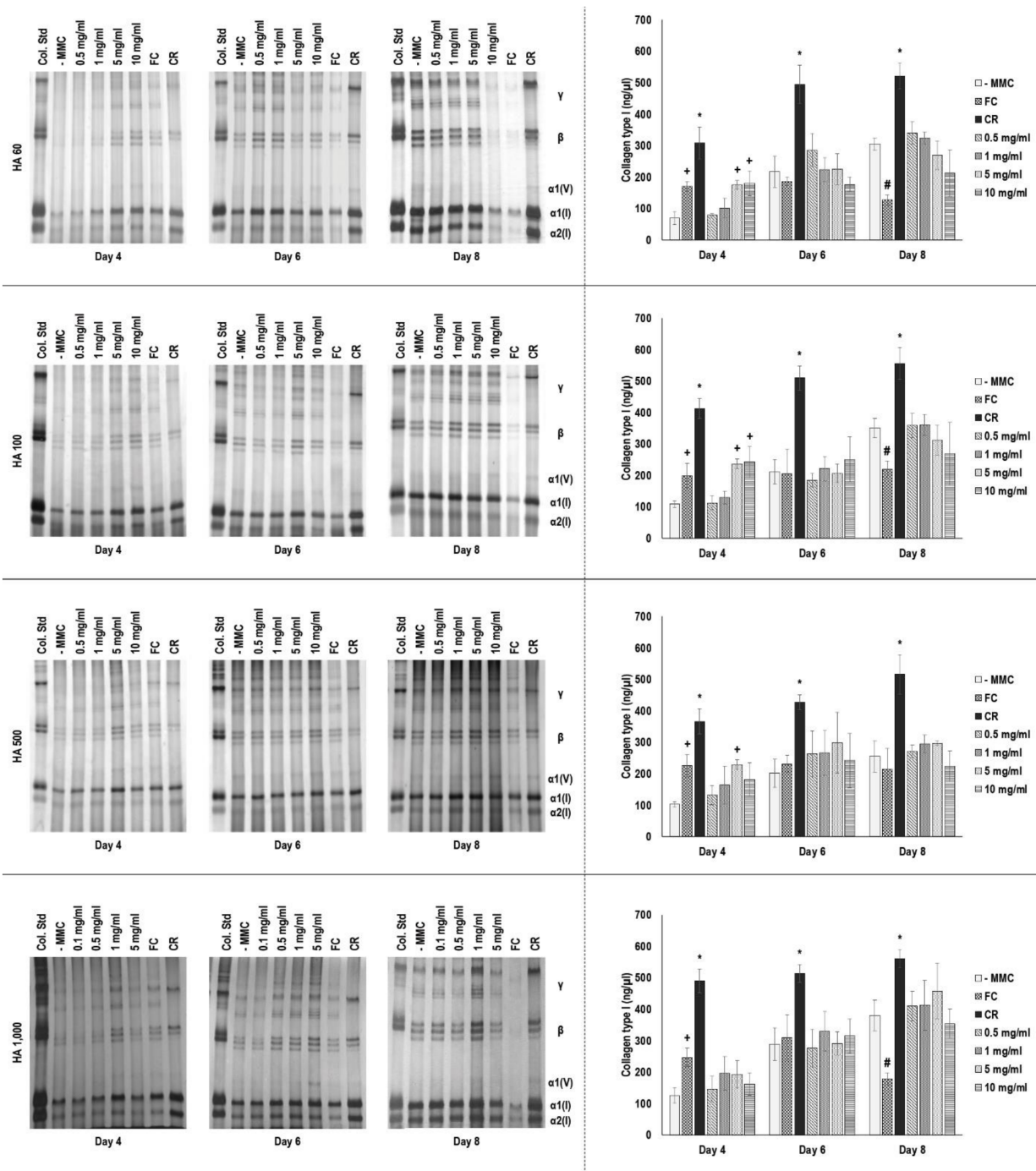


Figure 1. SDS-PAGE and complementary densitometry analyses revealed that carrageenan induced the highest ($p < 0.05$) collagen type I deposition at all timepoints. * indicates significantly ($p < 0.05$) higher deposition among all groups at a given timepoint. + indicates significantly ($p < 0.05$) higher deposition than the non-macromolecular crowding (MMC) control group at a given timepoint. # indicates significantly ($p < 0.05$) lower deposition than the non-MMC control group at a given timepoint.

3.7. Immunocytochemistry Assessment

Immunocytochemistry (Figure 2) and complementary fluorescence intensity (Figure S7A) analyses for collagen type I revealed that carrageenan induced the highest ($p < 0.001$) collagen type I deposition at all timepoints, Ficoll[®] induced higher ($p < 0.05$) collagen type I deposition than the non-MMC group only at days 4 and 6 and HA had no effect ($p > 0.05$) in collagen type I deposition at any timepoint, independently of the concentration and molecular weight.

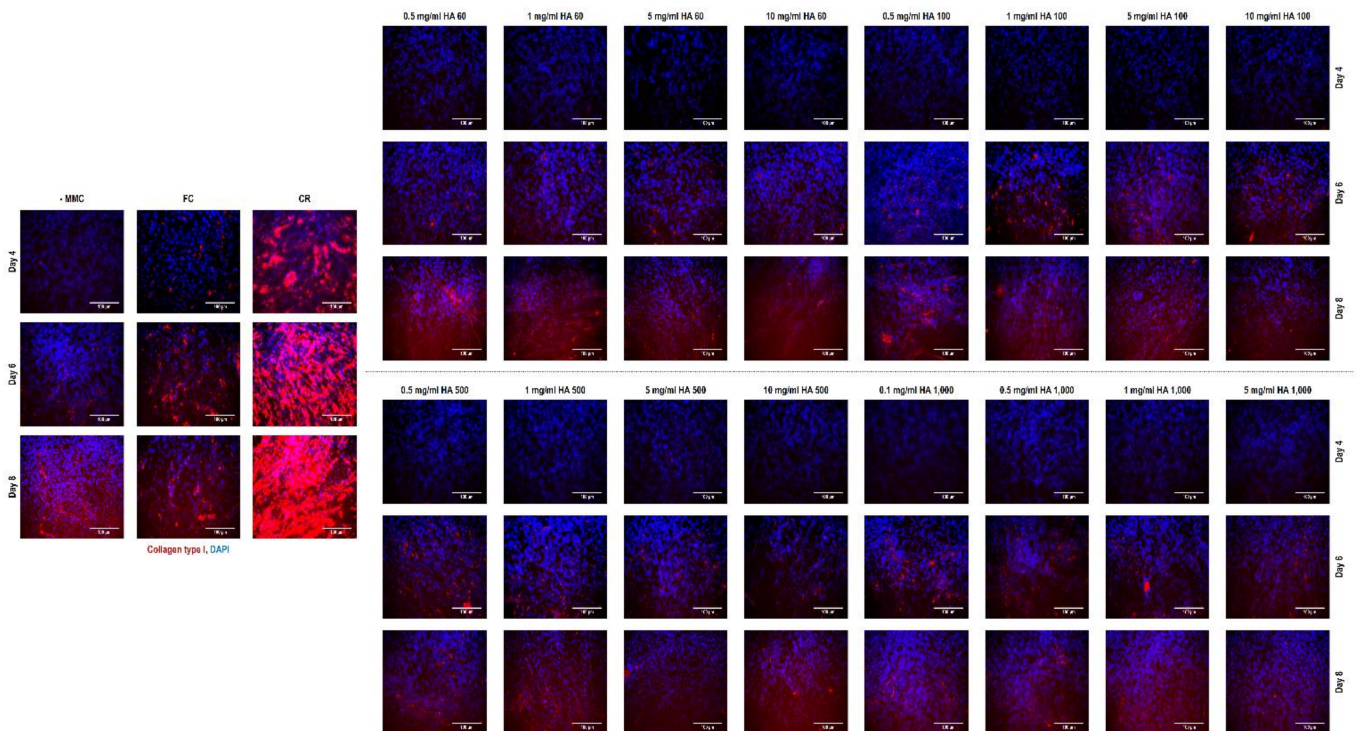


Figure 2. Immunocytochemistry analysis revealed that carrageenan induced the highest collagen type I deposition at all timepoints and at day 8 (longest timepoint assessed), no differences were observed between the non-MMC group and the Ficoll[®] and any of the HA groups.

Immunocytochemistry (Figure 3) and complementary fluorescence intensity (Figure S7B) analyses for collagen type III revealed that Ficoll[®] induced the highest ($p < 0.001$) collagen type III deposition (at day 6, the 10 mg/mL HA 500 kDa group was not significantly ($p > 0.05$) different to the Ficoll[®] group) and the carrageenan, the 10 mg/mL HA 60 kDa, the 5 mg/mL HA 100 kDa (only at day 6), the 10 mg/mL HA 100 kDa, the 5 and 10 mg/mL HA 500 kDa and the 5 mg/mL HA 1000 kDa groups induced higher ($p < 0.05$) collagen type III deposition than the non-MMC group at all timepoints.

Immunocytochemistry (Figure 4) and complementary fluorescence intensity (Figure S7C) analyses for collagen type IV revealed that Ficoll[®] induced the highest ($p < 0.001$) collagen type IV deposition and the carrageenan, the 10 mg/mL HA 60 kDa, the 10 mg/mL HA 100 kDa, the 10 mg/mL HA 500 kDa (only at days 6 and 8) and the 5 mg/mL HA 1000 kDa (only at days 6 and 8) groups induced higher ($p < 0.05$) collagen type IV deposition than the non-MMC group at all timepoints.

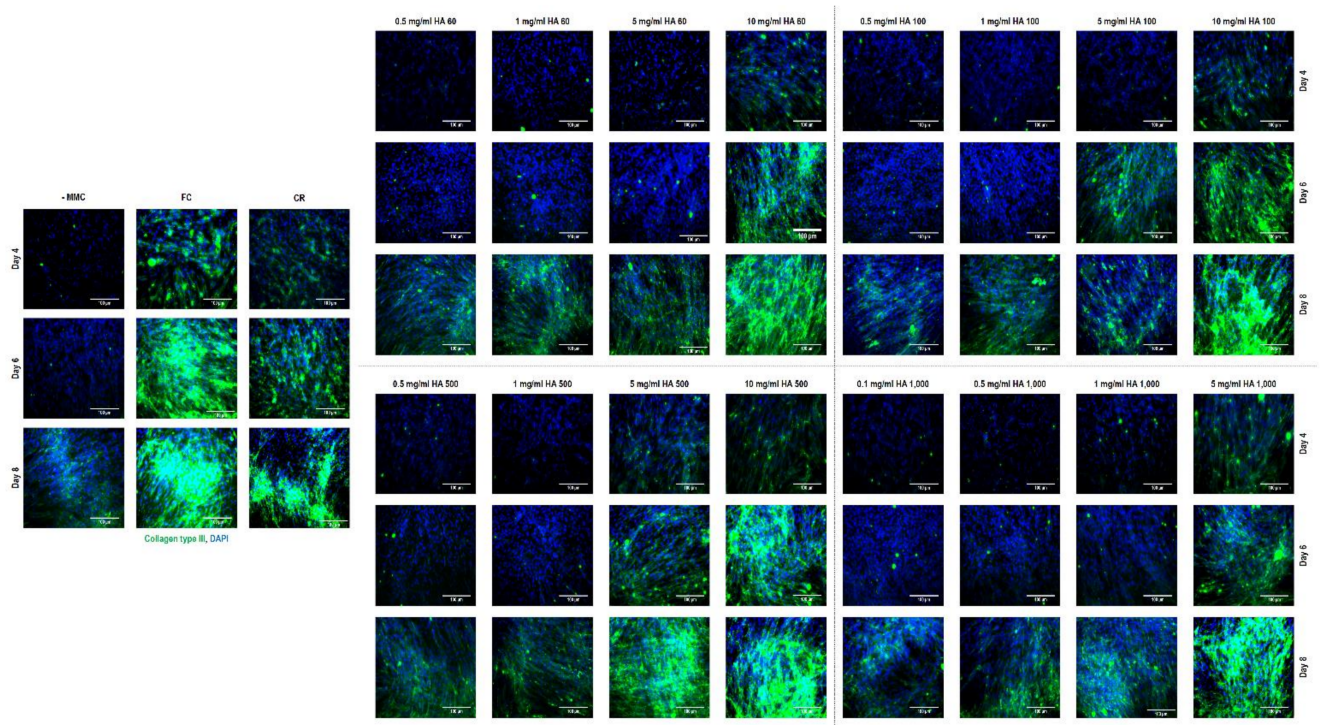


Figure 3. Immunocytochemistry analysis revealed that Ficoll® induced the highest collagen type III deposition at all timepoints and at day 8 (longest timepoint assessed), the carrageenan, the 10 mg/mL HA 60 kDa, the 10 mg/mL HA 100 kDa, the 5 and 10 mg/mL HA 500 kDa and the 5 mg/mL HA 1000 kDa induced significantly higher collagen type III deposition than the non-MMC group.

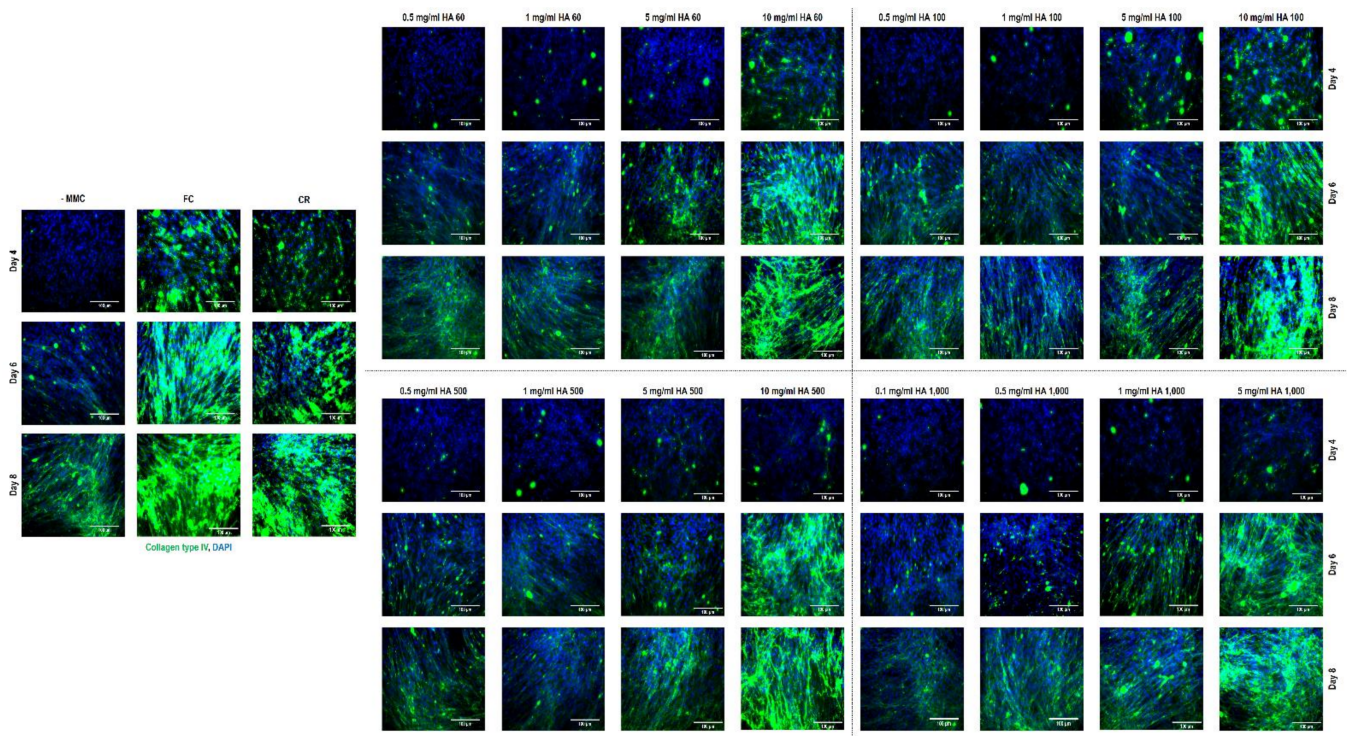


Figure 4. Immunocytochemistry analysis revealed that Ficoll® induced the highest collagen type IV deposition at all timepoints and at day 8 (longest timepoint assessed), the carrageenan, the 10 mg/mL HA 60 kDa, the 10 mg/mL HA 100 kDa, the 10 mg/mL HA 500 kDa and the 5 mg/mL HA 1000 kDa induced significantly higher collagen type IV deposition than the non-MMC group.

4. Discussion

In recent years, the use of MMC has been advocated for, for the accelerated development of tissue moduli for regenerative medicine [49] and drug discovery [50] purposes, as well as for the development of cell-derived matrices for effective cell expansion *ex vivo* [51] and as a quality control tool in cell culture media development [52]. Despite these significant strides, the optimal (with respect to the highest ECM deposition in the shortest period of time) MMC agent is still elusive. Among the various MMC agents, carrageenan has been comprehensively shown to induce the highest ECM deposition in the shortest period of time due to its negative charge and high polydispersity [13–15]. However, at the time of writing, carrageenan is only FDA-approved as a food additive [53]. In order, therefore, to capitalise on the immense power of MMC to accelerate the development of implantable tissue engineering devices, regulatory-compliant for medical applications macromolecules should be identified. With these in mind, herein we ventured to assess the potential of different concentrations of different molecular weight HAs as MMC agents. It is worth noting that the safety and efficacy of HA has been well-demonstrated in clinical practice (e.g., intra-articular viscosupplementation [54], aesthetic reconstruction of interdental papilla loss in anterior teeth [55], intra-dermal injections [56] and as dermal filler in photodamaged skin [57]) and it has been regulatory cleared (e.g., topical wound cream: 510(K) number: K172747 and treatment of pain in osteoarthritis: premarket approval number: P170016).

Starting with solubility assessment, we found a molecular weight-dependent solubility, with the 1000 kDa molecular weight HA able to remain soluble up to 5 mg/mL concentration, whilst the 10 kDa molecular weight HA was found to be soluble up to 200 mg/mL concentration. In accordance with our work, similar HA concentrations/molecular weights have been used in the literature as media supplements (e.g., 2 mg/mL 1800 kDa HA in human bone marrow stem cells [58]; 0.25–1.00 mg/mL 600–2000 kDa HA in human tenocyte cultures [59,60]; 0.5 and 5 mg/mL 1500 kDa HA in human neonatal fibroblast cultures [36]; 0.5, 1.0 and 2.0 mg/mL 30–1,300 kDa HA in calvarial mesenchymal cell (from 13 days old mouse embryos) cultures [61]; 0.1 and 0.5 mg/mL 500–730 kDa HA in human chondrocytes [62]; 0.5, 1 and 2 mg/mL 60 kDa and 900 kDa HA in rat calvarial-derived cell cultures [63]; 0.1 mg/mL 2000 and 3000 kDa HA in equine bone marrow stem cell chondrogenic differentiation cultures [64]; and 4 mg/mL 800 kDa HA in porcine bone marrow stem cell cultures [65]).

With respect to biophysical analysis, all molecules assessed had a negative charge; the high negative charge of carrageenan can be attributed to its sulphate content [66], and the FicolI[®], although it is considered to be non-ionic, is a rather heterogeneous in molecular weight macromolecule and has been demonstrated to contain negatively charged residues on about 50% of its macromolecular components [67], and the carboxyl groups of the glucuronic acid residues are negatively charged at physiological pH and ionic strength, making hyaluronic acid a negatively charged polyanionic macromolecule [68–70]. For the HA 100 kDa and the HA 500 kDa, a concentration-dependent zeta potential decrease and a hydrodynamic radius increase was observed as a function of increased concentration. This is in agreement with previous publications, where the charge was decreased and the mean particle size was increased as a function of increasing nanoparticle concentrations due to their aggregation in high concentrations [71–73]. Carrageenan, FicolI[®], HA 60 kDa, HA 100 kDa (only the 1 mg/mL concentration), HA 500 kDa and HA 1000 kDa exhibited a polydispersity index of > 0.7, which indicates a high degree of heterogeneity, due to broad size (i.e., polydisperse) distribution or agglomeration or aggregation of the particles of a population [74]. We attribute the observed differences in the polydispersity index of HA 100 kDa to experimental limitations of the method, as high sample concentrations (and therefore too high particle concentrations) result in multi-scattering or unpredictable agglomeration, whilst low sample concentrations (and therefore too dilute particle concentrations) may not generate enough light to analyse [72,73]. With respect to % fractional volume occupancy, only the 0.5 and 1 mg/mL HA 500 concentrations

and the 0.1 mg/mL HA 1000 concentration exhibited a % fraction volume occupancy below 60%, which is at the boundary of probability. Over the years, a diverse range of % fraction volume occupancy values have been reported in the literature using the method that we also used herein [47] (e.g., 5.2% for dextran sulphate 500 kDa [75]; 28% for a cocktail of dextran sulphate 10 kDa, Ficoll® 70 kDa and Ficoll® 400 kDa [51]; 9–54% for a Ficoll® 70 kDa and Ficoll® 400 kDa cocktail (subject to the concentration of each molecule in the solution) and polyvinylpyrrolidone 40 kDa and polyvinylpyrrolidone 360 kDa (subject to the concentration of each molecule in the respective solution) [32]; and >100% for highly sulphated seaweed polysaccharides, such as carrageenan, fucoidan, galactofucan, arabinogalactan and ulvan [15]). Although % fractional volume occupancy is frequently employed to predict the effectiveness of a macromolecule to occupy space/exclude volume in cell culture and consequently result in enhanced and accelerated ECM deposition, we believe that this approach should be treated with caution as the % fractional volume occupancy is calculated from the molecular weight and the hydrodynamic radius, based on the assumption that the molecule in question is spherical, which is not the case in real life (e.g., dextran is a ribbon-like or rod-like molecule, and Ficoll® is considered as a deformable sphere, as opposed to a compact sphere [76]).

Moving into basic cellular function analysis, none of the MMC agents assessed affected cell morphology and viability, whilst the Ficoll® at all timepoints, the carrageenan at day 8, the 10 mg/mL HA 100 kDa at day 8, the 10 mg/mL HA 500 kDa at day 6 and 8 and the 5 mg/mL HA 1000 kDa at day 8 induced reduced cell proliferation and increased metabolic activity in comparison to the non-MMC control group. Previous studies have shown Ficoll® and/or carrageenan to not affect human bone marrow stem cell morphology, viability and metabolic activity [49,77] (albeit, a non-significant decrease in metabolic activity has been reported for carrageenan [78] and a significant increase in proliferation has been reported for Ficoll® after 24 h [79], which may be asymptomatic), whilst in human adipose-derived stem cell (ADSC) cultures, carrageenan has been shown to not affect cell morphology and viability, but to increase cell proliferation and to decrease cell metabolic activity [15], and Ficoll® has been shown to affect cell morphology, to significantly increase metabolic activity only at day 1 and to significantly decrease DNA at days 4, 7 and 11 [80], in all cases, in comparison to the respective non-MMC group. In permanently differentiated cell cultures, Ficoll® has been shown to not affect the morphology, viability and metabolic activity of human corneal fibroblasts [31] and carrageenan has been shown to not affect the morphology, viability, metabolic activity and proliferation of human corneal fibroblasts [81] and human tenocytes [82]. With respect to HA, 2 mg/mL 1800 kDa HA supplementation in human bone marrow stem cells has been shown to not affect DNA content [58] and 1 µg/mL 850 kDa HA supplementation in human ADSCs has been shown to significantly increase cell proliferation (the 0.1 and 0.3 µg/mL concentrations; although they increased cell proliferation, the increase was not significant) and the 5 mg/mL concentration has been shown to decrease metabolic activity only at day 7 (longest timepoint assessed) and to not affect cell viability at any timepoint [83]. In permanently differentiated cell cultures, 0.25–1.00 mg/mL 600–2000 kDa HA supplementation has been shown to not affect human tenocyte morphology and to increase viability and proliferation in a dose-dependent manner [59,60]; 0.01, 0.1 and 1 mg/mL 800,000 viscometric average molecular weight (11.8–19.5 dL/g viscosity) HA supplementation has been shown to not affect rabbit chondrocyte (embedded in a collagen hydrogel) morphology and to increase cell proliferation (0.1 mg/mL HA induced the highest proliferation) [84]; 0.5 and 5 mg/mL 1500 kDa HA supplementation has been shown to not affect human neonatal fibroblast proliferation [36]; and 0.5–2 mg/mL 60 kDa HA and 0.5–1 mg/mL 900 kDa HA increased proliferation of calvarial rat-derived cells [63]. It is also worth noting that HA supplementation has also been shown to inhibit cell proliferation (e.g., 1–100 µg/mL 1000 and 1800 kDa HA negatively affected the proliferation of foetal rabbit skin fibroblasts [85] and rabbit synovial cells [86]; and 2 mg/mL 500, 800, 1600 and 3600 kDa inhibited rabbit tendon cell proliferation [87]).

Collectively, although a cell-dependent response to MMC is evidenced, an adverse effect in basic cellular functions cannot be noted.

SDS-PAGE and immunocytochemistry analyses revealed that the eADSCs were able to synthesise and deposit collagen types I, III and IV. All these ECM macromolecules are essential for physiological tissue development, function and healing; for example, collagen types I and III are the most abundant collagens in the human body, with collagen type I playing a crucial role in the structural and biomechanical integrity of tissues [88] and collagen type III regulating collagen type I fibrillogenesis and fibril diameter [89]. Collagen type IV is the most copious collagen in basement membranes and plays a crucial role in embryogenesis and wound healing, whilst minor structural differences can lead to pathophysiological [90]. Under MMC conditions, carrageenan induced the highest collagen type I deposition, which is in agreement with previous publications with a diverse range of cell populations (e.g., in human skin fibroblasts over Ficoll[®] 70 kDa, Ficoll[®] 400 kDa, Ficoll[®] 1000 kDa and cocktails thereof, dextran sulphate 10 kDa, dextran sulphate 100 kDa, dextran sulphate 500 kDa and cocktails thereof [14]; in human corneal fibroblasts over dextran sulphate 500 kDa [81]; in human lung and skin fibroblasts over dextran sulphate 500 kDa and a Ficoll[®] 70 kDa and Ficoll[®] 400 kDa cocktail [13]; in human bone marrow stem cells over a Ficoll[®] 70 kDa and Ficoll[®] 400 kDa cocktail [49]; and in human ADSCs over fucoidan, galactofucan, arabinogalactan and ulvan [15]). This superiority of carrageenan in inducing the highest ECM deposition has been attributed to its negative charge and high polydispersity [13,14]. With respect to Ficoll[®], the highest (over the non-MMC control) collagen type I deposition was only observed at day 4. Although one study has shown the Ficoll[®] cocktail to result in lower collagen deposition than the non-MMC group after 14 days in human neonatal fibroblast cultures [36], most studies have shown the Ficoll[®] cocktail to enhance collagen type I deposition in various cell populations (e.g., human skin fibroblasts [91], human corneal fibroblasts [31], human lung and skin fibroblasts [13], human bone marrow stem cells [79] and human ADSCs [80]), albeit at slower rates than sulphated polysaccharides [14,50]. Finally, HA had no effect on collagen type I deposition at any timepoint, independently of the concentration and molecular weight. With respect to the influence of increasing concentrations of a crowder in collagen deposition, previous studies have shown collagen deposition to be increased as a function of increasing carrageenan (for example) concentration (especially at early time points) [13,14,49]; above the optimal (with respect to enhanced and accelerated collagen deposition) concentration range, the concomitant increase in viscosity reduces reaction kinetics, as observed in protein folding/diffusion studies [92,93]. Thus, one would have expected increasing HA concentration, which resulted in an increased % fractional volume occupancy, to also result in increased collagen deposition. Considering though that polydispersity was not increased as a function of increasing HA concentration, and neither was the collagen deposition, we feel that this further substantiates our aforementioned claim with respect to the theoretical, as opposed to practical, nature of % fractional volume occupancy. With respect to the ability of HA to enhance and accelerate collagen type I deposition, our data are in both agreement (e.g., 10 mg/mL HA 2, 250 and 1000 kDa injected into full-thickness dermal wounds of aged mice did not increase collagen type I deposition [94], 50 mg/mL HA-12 saccharide units derived from HA 1700 kDa did not affect collagen synthesis in human skin fibroblasts [95], 100 mg/mL had no effect in collagen synthesis in foetal rabbit skin fibroblasts [85], 500 mg/mL HA (molecular weight was not stated) had no effect on collagen synthesis in human skin fibroblast cultures [96], 500 mg/mL HA 1600 kDa had no effect on the cell layer or the media collagen content in human skin fibroblast cultures [97], 500 and 5000 mg/mL HA 1500 kDa had a marginal (assessed via electrophoresis and Raman imaging) and no effect (assessed via immunocytochemistry), respectively, in collagen deposition in human neonatal fibroblast cultures [36]) and disagreement (e.g., 1 and 10 mg/mL HA 1000–1800 kDa increased collagen synthesis in foetal rabbit skin fibroblasts [85], and 1 and 10 mg/mL HA-12 saccharide units derived from HA 1700 kDa increased collagen synthesis in human skin fibroblasts [95]) with previous observations. With respect to collagen

type III and collagen type IV deposition, the Ficoll[®], carrageenan, 10 mg/mL HA 60 kDa, 10 mg/mL HA 100 kDa, 10 mg/mL HA 500 kDa, and 5 mg/mL HA 1000 kDa induced their highest deposition. Enhanced collagen type III and/or collagen type IV deposition with Ficoll[®] and/or carrageenan has been reported previously in human bone marrow stem cells [49,78], human corneal fibroblasts [31,81], human skin fibroblasts [13,98] and human tenocyte [82,99] cultures, but not in human ADSCs [15], human tenocytes, neonatal fibroblasts, adult fibroblasts, bone marrow stem cells [77] and human neonatal fibroblast [36] cultures. With respect to HA, 1, 10 and 50 mg/mL HA 1700 kDa and HA-12 and HA-880 saccharide units derived from HA 1700 kDa increased collagen type III synthesis in human skin fibroblast cultures [95], whilst 500 and 5000 mg/mL HA 1500 kDa had no effect on collagen type III and collagen type IV deposition in human neonatal fibroblast cultures [36]. It is also worth noting that HAs of 2300 and 3000 to 5800 kDa had an inhibitory/cytotoxic effect on the monolayer in human skin fibroblast cultures, whilst 1000 mg/mL HA 500 to 1200 kDa increased collagen type III synthesis in human skin fibroblasts embedded within a collagen hydrogel, as was evidenced with Sirius red staining [100]. Further, 10 mg/mL HA 250 kDa increased collagen type III deposition in full-thickness dermal wounds of aged mice, whilst 10 mg/mL HA 2 and 1000 kDa had no effect [94]. It appears that a concentration cut-off exists in the literature for the high molecular weight HAs, with concentrations up to 50 mg/mL able to enhance collagen deposition, whilst concentrations higher than 50 mg/mL have no effect. In our case, the lowest concentration assessed was 100 mg/mL for all HAs molecular weights (60, 100, 500 and 1000 kDa). One can argue that concentrations below 50 mg/mL are outside of the MMC zone, but considering the very high water-binding capacity of HA (up to 6 L per g [37,38]), it may be actually possible to act as an MMC agent even at such low concentrations. One cannot also exclude that cell-specific biological events may be at play, considering that, through growth factor interaction and involvement in signalling cascades, sulphated polysaccharides have been shown to enhance the chondrogenic and osteogenic potential of stem cells [15,49,78], whilst non-sulphated polysaccharides have been shown to enhance the adipogenic potential of stem cells [101,102]. Biochemical interactions can also be responsible for the observed results, as previous studies have shown mutual tropocollagen/HA steric exclusion [103,104].

5. Conclusions

In the quest for the optimal macromolecular crowder for enhanced and accelerated extracellular matrix deposition, herein we ventured to assess the potential of different concentrations and molecular weight hyaluronic acids. As carrageenan and Ficoll[®], customarily used crowding molecules, induced the highest collagen I, collagen III and collagen IV deposition, unless a biological benefit for hyaluronic acid is identified, we recommend their use as macromolecular crowding molecules for enhanced and accelerated extracellular matrix deposition.

Supplementary Materials: The following are available online at <https://www.mdpi.com/article/10.3390/cells10040859/s1>. Table S1: Qualitative HA solubility assessment as a function of molecular weight and concentration. ✓ indicates soluble; Figure S1: Experimental workflow of cell culture work and analysis; Figure S2: The extracted cells had the capacity to deposit calcium in osteogenic media, lipid droplets in adipogenic media and glycosaminoglycans in chondrogenic media; Figure S3: Bright field microscopy analysis after 4 days in culture revealed that up to 10 mg/mL concentrations of the HAs 60, 100 and 500 kDa and up to 5 mg/mL concentrations of HA 1000 kDa were completely soluble and allowed cell attachment and growth (black font); Figure S4: Bright field microscopy analysis revealed no apparent differences at any timepoint in cell morphology between the groups; Figure S5: Qualitative cell viability analysis revealed no apparent differences at any timepoint in cell viability between the groups; Figure S6: Quantitative cell viability analysis revealed no apparent differences at any timepoint in cell viability between the groups; Figure S7: Fluorescence intensity analyses revealed that carrageenan induced the highest ($p < 0.001$) collagen type I deposition

Author Contributions: S.G.-G. and D.I.Z. designed the study. S.G.-G. carried out most experiments and conducted data analysis. S.H.K. carried out chondrogenic analysis. N.D. and N.P. provided

the cells. D.I.Z., I.S., A.T., N.D. and N.P. supervised the work. S.G.-G. and D.I.Z. interpreted the findings and wrote the manuscript. All authors have read and agreed to the published version of the manuscript.

Funding: This work has received funding from the European Union’s Horizon 2020 research and innovation programme under the Marie Skłodowska-Curie, grant agreement No. 676338, the European Research Council (ERC) under the European Union’s Horizon 2020 research and innovation programme, grant agreement No. 866126 and the European Union’s Horizon 2020 research and innovation Widespread: Twinning programme, grant agreement No. 810850. This publication has emanated from research supported by grants from Science Foundation Ireland (SFI) under grant numbers 15/CDA/3629 and 19/FFP/6982 and Science Foundation Ireland (SFI) and European Regional Development Fund (ERDF) under grant number 13/RC/2073_2.

Institutional Review Board Statement: Not applicable.

Informed Consent Statement: Not applicable.

Data Availability Statement: Data are available from DIZ upon request.

Acknowledgments: Not applicable.

Conflicts of Interest: The authors declare no conflict of interest. The funders had no role in the design of the study; in the collection, analyses, or interpretation of data; in the writing of the manuscript; or in the decision to publish the results.

References

- Miyagawa, S.; Domae, K.; Yoshikawa, Y.; Fukushima, S.; Nakamura, T.; Saito, A.; Sakata, Y.; Hamada, S.; Toda, K.; Pak, K.; et al. Phase I clinical trial of autologous stem cell-sheet transplantation therapy for treating cardiomyopathy. *J. Am. Heart Assoc.* **2017**, *6*, e003918. [[CrossRef](#)]
- Sato, M.; Yamato, M.; Mitani, G.; Takagaki, T.; Hamahashi, K.; Nakamura, Y.; Ishihara, M.; Matoba, R.; Kobayashi, H.; Okano, T.; et al. Combined surgery and chondrocyte cell-sheet transplantation improves clinical and structural outcomes in knee osteoarthritis. *NPJ Regen Med.* **2019**, *4*, 4. [[CrossRef](#)]
- da Cruz, L.; Fynes, K.; Georgiadis, O.; Kerby, J.; Luo, Y.; Ahmado, A.; Vernon, A.; Daniels, J.; Nommiste, B.; Hasan, S.; et al. Phase 1 clinical study of an embryonic stem cell-derived retinal pigment epithelium patch in age-related macular degeneration. *Nat. Biotechnol.* **2018**, *36*, 328–337. [[CrossRef](#)]
- Hirsch, T.; Rothoefel, T.; Teig, N.; Bauer, J.; Pellegrini, G.; De Rosa, L.; Scaglione, D.; Reichelt, J.; Klausegger, A.; Kneisz, D.; et al. Regeneration of the entire human epidermis using transgenic stem cells. *Nature* **2017**, *551*, 327–332. [[CrossRef](#)] [[PubMed](#)]
- L’Heureux, N.; Dusserre, N.; Konig, G.; Victor, B.; Keire, P.; Wight, T.; Chronos, N.; Kyles, A.; Gregory, C.; Hoyt, G.; et al. Human tissue-engineered blood vessels for adult arterial revascularization. *Nat. Med.* **2006**, *12*, 361–365. [[CrossRef](#)] [[PubMed](#)]
- Hernandez-Segura, A.; Nehme, J.; Demaria, M. Hallmarks of cellular senescence. *Trends Cell Biol.* **2018**, *28*, 436–453. [[CrossRef](#)] [[PubMed](#)]
- Ten Ham, R.; Hövels, A.; Hoekman, J.; Frederix, G.; Leufkens, H.; Klungel, O.; Jedema, I.; Veld, S.; Nikolic, T.; Van Pel, M.; et al. What does cell therapy manufacturing cost? A framework and methodology to facilitate academic and other small-scale cell therapy manufacturing costings. *Cytotherapy* **2020**, *22*, 388–397. [[CrossRef](#)] [[PubMed](#)]
- Bettinger, C.; Langer, R.; Borenstein, J. Engineering substrate topography at the micro- and nanoscale to control cell function. *Angew. Chem. Int. Ed. Engl.* **2009**, *48*, 5406–5415. [[CrossRef](#)]
- Nemir, S.; West, J. Synthetic materials in the study of cell response to substrate rigidity. *Ann. Biomed. Eng.* **2010**, *38*, 2–20. [[CrossRef](#)] [[PubMed](#)]
- Mohyeldin, A.; Garzón-Muvdi, T.; Quiñones-Hinojosa, A. Oxygen in stem cell biology: A critical component of the stem cell niche. *Cell Stem Cell* **2010**, *7*, 150–161. [[CrossRef](#)]
- Delaine-Smith, R.; Reilly, G. The effects of mechanical loading on mesenchymal stem cell differentiation and matrix production. *Vitam. Horm.* **2011**, *87*, 417–480.
- Lee, D.; Kim, D.; Cho, J. Role of growth factors in hematopoietic stem cell niche. *Cell Biol. Toxicol.* **2020**, *36*, 131–144. [[CrossRef](#)]
- Satyam, A.; Kumar, P.; Fan, X.; Gorelov, A.; Rochev, Y.; Joshi, L.; Peinado, H.; Lyden, D.; Thomas, B.; Rodriguez, B.; et al. Macromolecular crowding meets tissue engineering by self-assembly: A paradigm shift in regenerative medicine. *Adv. Mater.* **2014**, *26*, 3024–3034. [[CrossRef](#)]
- Gaspar, D.; Fuller, K.P.; Zeugolis, D.I. Polydispersity and negative charge are key modulators of extracellular matrix deposition under macromolecular crowding conditions. *Acta Biomater.* **2019**, *88*, 197–210. [[CrossRef](#)]
- De Pieri, A.; Rana, S.; Korntner, S.; Zeugolis, D. Seaweed polysaccharides as macromolecular crowding agents. *Int. J. Biol. Macromol.* **2020**, *164*, 434–446. [[CrossRef](#)] [[PubMed](#)]
- Miyahara, M.; Njieha, F.; Prockop, D. Formation of collagen fibrils in vitro by cleavage of procollagen with procollagen proteinases. *J. Biol. Chem.* **1982**, *257*, 8442–8448. [[CrossRef](#)]

17. Zeugolis, D. Bioinspired in vitro microenvironments to control cell fate: Focus on macromolecular crowding. *Am. J. Physiol. Cell Physiol.* **2021**, submitted.
18. Kuznetsova, I.; Zaslavsky, B.; Breydo, L.; Turoverov, K.; Uversky, V. Beyond the excluded volume effects: Mechanistic complexity of the crowded milieu. *Molecules* **2015**, *20*, 1377–1409. [[CrossRef](#)] [[PubMed](#)]
19. Ando, T.; Skolnick, J. Crowding and hydrodynamic interactions likely dominate in vivo macromolecular motion. *Proc. Natl. Acad. Sci. USA* **2010**, *107*, 18457–18462. [[CrossRef](#)] [[PubMed](#)]
20. Miyoshi, D.; Sugimoto, N. Molecular crowding effects on structure and stability of DNA. *Biochimie* **2008**, *90*, 1040–1051. [[CrossRef](#)]
21. Ramisetty, S.; Langlete, P.; Lale, R.; Dias, R. In vitro studies of DNA condensation by bridging protein in a crowding environment. *Int. J. Biol. Macromol.* **2017**, *103*, 845–853. [[CrossRef](#)]
22. Akabayov, B.; Akabayov, S.; Lee, S.; Wagner, G.; Richardson, C. Impact of macromolecular crowding on DNA replication. *Nat. Commun.* **2013**, *4*, 1615. [[CrossRef](#)]
23. Chung, S.; Lerner, E.; Jin, Y.; Kim, S.; Alhadid, Y.; Grimaud, L.; Zhang, I.; Knobler, C.; Gelbart, W.; Weiss, S. The effect of macromolecular crowding on single-round transcription by Escherichia coli RNA polymerase. *Nucleic Acids Res.* **2019**, *47*, 440–1450. [[CrossRef](#)]
24. Wirth, A.; Gruebele, M. Quinary protein structure and the consequences of crowding in living cells: Leaving the test-tube behind. *Bioessays* **2013**, *35*, 984–993. [[CrossRef](#)]
25. Christiansen, A.; Wang, Q.; Cheung, M.; Wittung-Stafshede, P. Effects of macromolecular crowding agents on protein folding in vitro and in silico. *Biophys. Rev.* **2013**, *5*, 137–145. [[CrossRef](#)] [[PubMed](#)]
26. Guseman, A.; Speer, S.; Perez Goncalves, G.; Pielak, G. Surface charge modulates protein-protein interactions in physiologically relevant environments. *Biochemistry* **2018**, *57*, 1681–1684. [[CrossRef](#)] [[PubMed](#)]
27. Kang, H.; Toan, N.; Hyeon, C.; Thirumalai, D. Unexpected swelling of stiff DNA in a polydisperse crowded environment. *J. Am. Chem. Soc.* **2015**, *137*, 10970–10978. [[CrossRef](#)] [[PubMed](#)]
28. Sharp, K.A. Analysis of the size dependence of macromolecular crowding shows that smaller is better. *Proc. Natl. Acad. Sci. USA* **2015**, *112*, 7990–7995. [[CrossRef](#)] [[PubMed](#)]
29. Skóra, T.; Vaghefikia, F.; Fitter, J.; Kondrat, S. Macromolecular crowding: How shape and interactions affect diffusion. *J. Phys. Chem. B* **2020**, *124*, 7537–7543. [[CrossRef](#)] [[PubMed](#)]
30. von Bülow, S.; Siggel, M.; Linke, M.; Hummer, G. Dynamic cluster formation determines viscosity and diffusion in dense protein solutions. *Proc. Natl. Acad. Sci. USA* **2019**, *116*, 9843–9852. [[CrossRef](#)]
31. Kumar, P.; Satyam, A.; Fan, X.; Collin, E.; Rochev, Y.; Rodriguez, B.J.; Gorelov, A.; Dillon, S.; Joshi, L.; Raghunath, M.; et al. Macromolecularly crowded in vitro microenvironments accelerate the production of extracellular matrix-rich supramolecular assemblies. *Sci. Rep.* **2015**, *5*, 8729. [[CrossRef](#)] [[PubMed](#)]
32. Rashid, R.; Lim, N.; Chee, S.; Png, S.; Wohland, T.; Raghunath, M. Novel use for polyvinylpyrrolidone as a macromolecular crowder for enhanced extracellular matrix deposition and cell proliferation. *Tissue Eng. Part C Methods* **2014**, *20*, 994–1002. [[CrossRef](#)]
33. McKim, J.M.; Willoughby, J.A.; Blakemore, W.R.; Weiner, M.L. A critical review of “A randomized trial of the effects of the no-carrageenan diet on ulcerative colitis disease activity (Nutr. Healthy Aging. **2017**, *4*, 181–192).”. *J. Nutr. Health Aging* **2019**, *5*, 149–158. [[CrossRef](#)]
34. Shang, Q.; Sun, W.; Shan, X.; Jiang, H.; Cai, C.; Hao, J.; Li, G.; Yu, G. Carrageenan-induced colitis is associated with decreased population of anti-inflammatory bacterium, Akkermansia muciniphila, in the gut microbiota of C57BL/6J mice. *Toxicol. Lett.* **2017**, *279*, 87–95. [[CrossRef](#)]
35. Mi, Y.; Chin, Y.X.; Cao, W.X.; Chang, Y.G.; Lim, P.E.; Xue, C.H.; Tang, Q.J. Native κ-carrageenan induced-colitis is related to host intestinal microecology. *Int. J. Biol. Macromol.* **2020**, *147*, 284–294. [[CrossRef](#)] [[PubMed](#)]
36. Shendi, D.; Marzi, J.; Linthicum, W.; Rickards, A.J.; Dolivo, D.M.; Keller, S.; Kaus, M.A.; Wen, Q.; McDevitt, T.C.; Dominko, T.; et al. Hyaluronic acid as a macromolecular crowding agent for production of cell-derived matrices. *Acta Biomater.* **2019**, *100*, 292–305. [[CrossRef](#)]
37. Majewski, G.; Rodan, K.; Fields, K.; Falla, T. Characterization of bound water in skin hydrators prepared with and without a 3D3P interpenetrating polymer network. *Skin Res. Technol.* **2019**, *25*, 150–157. [[CrossRef](#)] [[PubMed](#)]
38. Papakonstantinou, E.; Roth, M.; Karakiulakis, G. Hyaluronic acid: A key molecule in skin aging. *Dermato-Endocrinol.* **2012**, *4*, 253–258. [[CrossRef](#)] [[PubMed](#)]
39. Cowman, M.K. Hyaluronan and hyaluronan fragments. *Adv. Carbohydr. Chem. Biochem.* **2017**, *74*, 1–59. [[CrossRef](#)]
40. Uphoff, C.C.; Drexler, H.G. Detection of Mycoplasma contamination in cell cultures. *Curr. Protoc. Mol. Biol.* **2014**, *106*, 1–14. [[CrossRef](#)]
41. Ranera, B.; Remacha, A.R.; Alvarez-Arguedas, S.; Romero, A.; Vazquez, F.J.; Zaragoza, P.; Martin-Burriel, I.; Rodellar, C. Effect of hypoxia on equine mesenchymal stem cells derived from bone marrow and adipose tissue. *BMC Vet. Res.* **2012**, *8*, 142. [[CrossRef](#)]
42. Ranera, B.; Lyahyai, J.; Romero, A.; Vazquez, F.J.; Remacha, A.R.; Bernal, M.L.; Zaragoza, P.; Rodellar, C.; Martin-Burriel, I. Immunophenotype and gene expression profiles of cell surface markers of mesenchymal stem cells derived from equine bone marrow and adipose tissue. *Vet. Immunol. Immunopathol.* **2011**, *144*, 147–154. [[CrossRef](#)]

43. Maia, L.; Landim-Alvarenga, F.C.; Da Mota, L.S.; De Assis Golim, M.; Laufer-Amorim, R.; De Vita, B.; Barberini, D.J.; Listoni, A.J.; De Moraes, C.N.; Heckler, M.C.; et al. Immunophenotypic, immunocytochemistry, ultrastructural, and cytogenetic characterization of mesenchymal stem cells from equine bone marrow. *Microsc. Res. Tech.* **2013**, *76*, 618–624. [[CrossRef](#)]
44. Barberini, D.J.; Freitas, N.P.; Magnoni, M.S.; Maia, L.; Listoni, A.J.; Heckler, M.C.; Sudano, M.J.; Golim, M.A.; da Cruz Landim-Alvarenga, F.; Amorim, R.M. Equine mesenchymal stem cells from bone marrow, adipose tissue and umbilical cord: Immunophenotypic characterization and differentiation potential. *Stem Cell Res. Ther.* **2014**, *5*, 25. [[CrossRef](#)]
45. Fulber, J.; Maria, D.A.; da Silva, L.C.; Massoco, C.O.; Agreste, F.; Baccarin, R.Y. Comparative study of equine mesenchymal stem cells from healthy and injured synovial tissues: An in vitro assessment. *Stem Cell Res. Ther.* **2016**, *7*, 35. [[CrossRef](#)]
46. Shikh Alsook, M.K.; Gabriel, A.; Piret, J.; Waroux, O.; Tonus, C.; Connan, D.; Baise, E.; Antoine, N. Tissues from equine cadaver ligaments up to 72 hours of post-mortem: A promising reservoir of stem cells. *Stem Cell Res. Ther.* **2015**, *6*, 253. [[CrossRef](#)] [[PubMed](#)]
47. Chen, C.; Loe, F.; Blocki, A.; Peng, Y.; Raghunath, M. Applying macromolecular crowding to enhance extracellular matrix deposition and its remodeling in vitro for tissue engineering and cell-based therapies. *Adv. Drug Deliv. Rev.* **2011**, *63*, 277–290. [[CrossRef](#)] [[PubMed](#)]
48. Capella-Monsonis, H.; Coentro, J.Q.; Graceffa, V.; Wu, Z.; Zeugolis, D.I. An experimental toolbox for characterization of mammalian collagen type I in biological specimens. *Nat. Protoc.* **2018**, *13*, 507–529. [[CrossRef](#)] [[PubMed](#)]
49. Cigognini, D.; Gaspar, D.; Kumar, P.; Satyam, A.; Alagesan, S.; Sanz-Nogues, C.; Griffin, M.; O'Brien, T.; Pandit, A.; Zeugolis, D.I. Macromolecular crowding meets oxygen tension in human mesenchymal stem cell culture—A step closer to physiologically relevant in vitro organogenesis. *Sci. Rep.* **2016**, *6*, 30746. [[CrossRef](#)]
50. Chen, C.Z.; Peng, Y.X.; Wang, Z.B.; Fish, P.V.; Kaar, J.L.; Koepsel, R.R.; Russell, A.J.; Lareu, R.R.; Raghunath, M. The Scar-in-a-Jar: Studying potential antifibrotic compounds from the epigenetic to extracellular level in a single well. *Br. J. Pharmacol.* **2009**, *158*, 1196–1209. [[CrossRef](#)]
51. Prewitz, M.C.; Stißel, A.; Friedrichs, J.; Träber, N.; Vogler, S.; Bornhäuser, M.; Werner, C. Extracellular matrix deposition of bone marrow stroma enhanced by macromolecular crowding. *Biomaterials* **2015**, *73*, 60–69. [[CrossRef](#)]
52. Graceffa, V.; Zeugolis, D.I. Macromolecular crowding as a means to assess the effectiveness of chondrogenic media. *J. Tissue Eng. Regen Med.* **2019**, *13*, 217–231. [[CrossRef](#)]
53. FDA. *Food Additives Permitted for Direct Addition to Food for Human Consumption. Section 172.620: Carrageenan*; US Food & Drug Administration: Washington, DC, USA, 2019.
54. Papalia, R.; Russo, F.; Torre, G.; Albo, E.; Grimaldi, V.; Papalia, G.; Sterzi, S.; Vadalà, G.; Bressi, F.; Denaro, V. Hybrid hyaluronic acid versus high molecular weight hyaluronic acid for the treatment of osteoarthritis in obese patients. *J. Biol. Regul. Homeost. Agents* **2017**, *31*, 103–109.
55. Awartani, F.; Tatakis, D. Interdental papilla loss: Treatment by hyaluronic acid gel injection: A case series. *Clin. Oral Investig.* **2016**, *20*, 1775–1780. [[CrossRef](#)]
56. Cavallini, M.; Papagni, M.; Ryder, T.; Patalano, M. Skin quality improvement with VYC-12, a new injectable hyaluronic acid: Objective results using digital analysis. *Dermatol. Surg.* **2019**, *45*, 1598–1604. [[CrossRef](#)]
57. Wang, F.; Garza, L.A.; Kang, S.; Varani, J.; Orringer, J.S.; Fisher, G.J.; Voorhees, J.J. In vivo stimulation of de novo collagen production caused by cross-linked hyaluronic acid dermal filler injections in photodamaged human skin. *Arch. Dermatol.* **2007**, *143*, 155–163. [[CrossRef](#)] [[PubMed](#)]
58. Monaco, G.; El Haj, A.; Alini, M.; Stoddart, M. Sodium hyaluronate supplemented culture media as a new hMSC chondrogenic differentiation media-model for in vitro/ex vivo screening of potential cartilage repair therapies. *Front. Bioeng. Biotechnol.* **2020**, *8*, 243. [[CrossRef](#)]
59. Gallorini, M.; Berardi, A.C.; Berardocco, M.; Gissi, C.; Maffulli, N.; Cataldi, A.; Oliva, F. Hyaluronic acid increases tendon derived cell viability and proliferation in vitro: Comparative study of two different hyaluronic acid preparations by molecular weight. *Muscles Ligaments Tendons J.* **2017**, *7*, 208–214. [[CrossRef](#)] [[PubMed](#)]
60. Osti, L.; Berardocco, M.; di Giacomo, V.; Di Bernardo, G.; Oliva, F.; Berardi, A. Hyaluronic acid increases tendon derived cell viability and collagen type I expression in vitro: Comparative study of four different hyaluronic acid preparations by molecular weight. *BMC Musculoskelet Disord.* **2015**, *16*, 284. [[CrossRef](#)] [[PubMed](#)]
61. Pilloni, A.; Bernard, G.W. The effect of hyaluronan on mouse intramembranous osteogenesis in vitro. *Cell Tissue Res.* **1998**, *294*, 323–333. [[CrossRef](#)]
62. Karna, E.; Miltik, W.; Palka, J.A.; Jarzabek, K.; Wolczynski, S. Hyaluronic acid counteracts interleukin-1-induced inhibition of collagen biosynthesis in cultured human chondrocytes. *Pharmacol. Res.* **2006**, *54*, 275–281. [[CrossRef](#)]
63. Huang, L.; Cheng, Y.Y.; Koo, P.L.; Lee, K.M.; Qin, L.; Cheng, J.C.; Kumta, S.M. The effect of hyaluronan on osteoblast proliferation and differentiation in rat calvarial-derived cell cultures. *J. Biomed. Mater. Res. A* **2003**, *66*, 880–884. [[CrossRef](#)]
64. Hegewald, A.A.; Ringe, J.; Bartel, J.; Kruger, I.; Notter, M.; Barnewitz, D.; Kaps, C.; Sittinger, M. Hyaluronic acid and autologous synovial fluid induce chondrogenic differentiation of equine mesenchymal stem cells: A preliminary study. *Tissue Cell* **2004**, *36*, 431–438. [[CrossRef](#)]
65. Zou, L.; Zou, X.; Chen, L.; Li, H.; Mygind, T.; Kassem, M.; Bunker, C. Effect of hyaluronan on osteogenic differentiation of porcine bone marrow stromal cells in vitro. *J. Orthop. Res. Off. Publ. Orthop. Res. Soc.* **2008**, *26*, 713–720. [[CrossRef](#)]
66. Li, L.; Ni, R.; Shao, Y.; Mao, S. Carrageenan and its applications in drug delivery. *Carbohydr. Polym.* **2014**, *103*, 1–11. [[CrossRef](#)]

67. Zhu, Y.; Potschka, M.; Dubin, P.; Cai, C.H. A method for the quantitation of charge by size exclusion chromatography demonstrated with components of ficoll 400. *Macromol. Chem. Phys.* **2001**, *202*, 61–72. [[CrossRef](#)]
68. Larrañeta, E.; Henry, M.; Irwin, N.; Trotter, J.; Perminova, A.; Donnelly, R. Synthesis and characterization of hyaluronic acid hydrogels crosslinked using a solvent-free process for potential biomedical applications. *Carbohydr. Polym.* **2018**, *181*, 1194–1205. [[CrossRef](#)] [[PubMed](#)]
69. Snetkov, P.; Zakharova, K.; Morozkina, S.; Olekhovich, R.; Uspenskaya, M. Hyaluronic acid: The influence of molecular weight on structural, physical, physico-chemical, and degradable properties of biopolymer. *Polymers* **2020**, *12*, 1800. [[CrossRef](#)] [[PubMed](#)]
70. Hascall, V.; Esko, J. Hyaluronan. In *Essentials of Glycobiology*, 3rd ed.; Varki, A., Cummings, R., Esko, J., Stanley, P., Hart, G., Aebi, M., Darvill, A., Kinoshita, T., Packer, N., Prestegard, J., et al., Eds.; Cold Spring Harbor Laboratory Press: Cold Spring Harbor, NY, USA, 2017.
71. Tantra, R.; Schulze, P.; Quincey, P. Effect of nanoparticle concentration on zeta-potential measurement results and reproducibility. *Particuology* **2010**, *8*, 279–285. [[CrossRef](#)]
72. Bhattacharjee, S. DLS and zeta potential—What they are and what they are not? *J. Control. Release Off. J. Control. Release Soc.* **2016**, *235*, 337–351. [[CrossRef](#)]
73. Panchal, J.; Kotarek, J.; Marszal, E.; Topp, E.M. Analyzing subvisible particles in protein drug products: A comparison of dynamic light scattering (DLS) and resonant mass measurement (RMM). *AAPS J.* **2014**, *16*, 440–451. [[CrossRef](#)]
74. Mudalige, T.; Qu, H.; Van Haute, D.; Ansar, S.M.; Paredes, A.; Ingle, T. Chapter 11—Characterization of nanomaterials: Tools and challenges. In *Nanomaterials for Food Applications*; López Rubio, A., Fabra Rovira, M.J., Martínez Sanz, M., Gómez-Mascaraque, L.G., Eds.; Elsevier: Amsterdam, The Netherlands, 2019; pp. 313–353. [[CrossRef](#)]
75. Lareu, R.R.; Subramhanya, K.H.; Peng, Y.; Benny, P.; Chen, C.; Wang, Z.; Rajagopalan, R.; Raghunath, M. Collagen matrix deposition is dramatically enhanced in vitro when crowded with charged macromolecules: The biological relevance of the excluded volume effect. *FEBS Lett.* **2007**, *581*, 2709–2714. [[CrossRef](#)]
76. Shahid, S.; Hassan, M.; Islam, A.; Ahmad, F. Size-dependent studies of macromolecular crowding on the thermodynamic stability, structure and functional activity of proteins: In vitro and in silico approaches. *Biochim. Biophys. Acta Gen. Subj.* **2017**, *1861*, 178–197. [[CrossRef](#)] [[PubMed](#)]
77. Gaspar, D.; Ryan, C.N.M.; Zeugolis, D.I. Multifactorial bottom-up bioengineering approaches for the development of living tissue substitutes. *FASEB J.* **2019**, *33*, 5741–5754. [[CrossRef](#)]
78. Graceffa, V.; Zeugolis, D.I. Carrageenan enhances chondrogenesis and osteogenesis in human bone marrow stem cell culture. *Eur. Cell Mater.* **2019**, *37*, 310–332. [[CrossRef](#)] [[PubMed](#)]
79. Zeiger, A.S.; Loe, F.C.; Li, R.; Raghunath, M.; Van Vliet, K.J. Macromolecular crowding directs extracellular matrix organization and mesenchymal stem cell behavior. *PLoS ONE* **2012**, *7*, e37904. [[CrossRef](#)] [[PubMed](#)]
80. Patrikoski, M.; Lee, M.H.C.; Mäkinen, L.; Ang, X.M.; Mannerström, B.; Raghunath, M.; Miettinen, S. Effects of macromolecular crowding on human adipose stem cell culture in fetal bovine serum, human serum, and defined xeno-free/serum-free conditions. *Stem Cells Int.* **2017**, *2017*, 6909163. [[CrossRef](#)]
81. Kumar, P.; Satyam, A.; Fan, X.; Rochev, Y.; Rodriguez, B.J.; Gorelov, A.; Joshi, L.; Raghunath, M.; Pandit, A.; Zeugolis, D.I. Accelerated development of supramolecular corneal stromal-like assemblies from corneal fibroblasts in the presence of macromolecular crowders. *Tissue Eng. Part C Methods* **2015**, *21*, 660–670. [[CrossRef](#)]
82. Tsiapalis, D.; De Pieri, A.; Spanoudes, K.; Sallent, I.; Kearns, S.; Kelly, J.L.; Raghunath, M.; Zeugolis, D.I. The synergistic effect of low oxygen tension and macromolecular crowding in the development of extracellular matrix-rich tendon equivalents. *Biofabrication* **2020**, *12*, 025018. [[CrossRef](#)]
83. Moreno, A.; Martínez, A.; Olmedillas, S.; Bello, S.; de Miguel, F. Hyaluronic acid effect on adipose-derived stem cells. Biological in vitro evaluation. *Rev. Esp. Cirugía Ortop. Traumatol.* **2015**, *59*, 215–221. [[CrossRef](#)]
84. Kawasaki, K.; Ochi, M.; Uchio, Y.; Adachi, N.; Matsusaki, M. Hyaluronic acid enhances proliferation and chondroitin sulfate synthesis in cultured chondrocytes embedded in collagen gels. *J. Cell Physiol.* **1999**, *179*, 142–148. [[CrossRef](#)]
85. Mast, B.A.; Diegelmann, R.F.; Krummel, T.M.; Cohen, I.K. Hyaluronic acid modulates proliferation, collagen and protein synthesis of cultured fetal fibroblasts. *Matrix* **1993**, *13*, 441–446. [[CrossRef](#)]
86. Goldberg, R.L.; Toole, B.P. Hyaluronate inhibition of cell proliferation. *Arthritis Rheum.* **1987**, *30*, 769–778. [[CrossRef](#)] [[PubMed](#)]
87. Wiig, M.; Abrahamsson, S.O.; Lundborg, G. Effects of hyaluronan on cell proliferation and collagen synthesis: A study of rabbit flexor tendons in vitro. *J. Hand. Surg. Am.* **1996**, *21*, 599–604. [[CrossRef](#)]
88. Sorushanova, A.; Delgado, L.M.; Wu, Z.; Shologu, N.; Kshirsagar, A.; Raghunath, R.; Mullen, A.M.; Bayon, Y.; Pandit, A.; Raghunath, M.; et al. The collagen suprafamily: From biosynthesis to advanced biomaterial development. *Adv. Mater.* **2019**, *31*, 1801651. [[CrossRef](#)] [[PubMed](#)]
89. Liu, X.; Wu, H.; Byrne, M.; Krane, S.; Jaenisch, R. Type III collagen is crucial for collagen I fibrillogenesis and for normal cardiovascular development. *Proc. Natl. Acad. Sci. USA* **1997**, *94*, 1852–1856. [[CrossRef](#)] [[PubMed](#)]
90. Abreu-Velez, A.; Howard, M. Collagen IV in normal skin and in pathological processes. *N. Am. J. Med. Sci.* **2012**, *4*, 1–8. [[CrossRef](#)] [[PubMed](#)]
91. Graham, J.; Raghunath, M.; Vogel, V. Fibrillar fibronectin plays a key role as nucleator of collagen I polymerization during macromolecular crowding-enhanced matrix assembly. *Biomater. Sci.* **2019**, *7*, 4519–4535. [[CrossRef](#)]

92. Lee, C.; Bird, S.; Shaw, M.; Jean, L.; Vaux, D. Combined effects of agitation, macromolecular crowding, and interfaces on amyloidogenesis. *J. Biol. Chem.* **2012**, *287*, 38006–38019. [[CrossRef](#)]
93. Chen, E.; Kliger, D. Time-resolved linear dichroism measurements of carbonmonoxy myoglobin as a probe of the microviscosity in crowded environments. *J. Phys. Chem. B* **2017**, *121*, 7064–7074. [[CrossRef](#)]
94. Damodarasamy, M.; Johnson, R.S.; Bentov, I.; MacCoss, M.J.; Vernon, R.B.; Reed, M.J. Hyaluronan enhances wound repair and increases collagen III in aged dermal wounds. *Wound Repair Regen* **2014**, *22*, 521–526. [[CrossRef](#)] [[PubMed](#)]
95. David-Raoudi, M.; Tranchepain, F.; Deschrevel, B.; Vincent, J.C.; Bogdanowicz, P.; Boumediene, K.; Pujol, J.P. Differential effects of hyaluronan and its fragments on fibroblasts: Relation to wound healing. *Wound Repair Regen* **2008**, *16*, 274–287. [[CrossRef](#)]
96. Donejko, M.; Przylipiak, A.; Rysiak, E.; Głuszuk, K.; Surazyński, A. Influence of caffeine and hyaluronic acid on collagen biosynthesis in human skin fibroblasts. *Drug Des. Devel. Ther.* **2014**, *8*, 1923–1928. [[PubMed](#)]
97. Croce, M.; Dyne, K.; Boraldi, F.; Quaglino, D.; Cetta, G.; Tiozzo, R.; Pasquali Ronchetti, I. Hyaluronan affects protein and collagen synthesis by in vitro human skin fibroblasts. *Tissue Cell* **2001**, *33*, 326–331. [[CrossRef](#)] [[PubMed](#)]
98. Satyam, A.; Kumar, P.; Cigognini, D.; Pandit, A.; Zeugolis, D.I. Low, but not too low, oxygen tension and macromolecular crowding accelerate extracellular matrix deposition in human dermal fibroblast culture. *Acta Biomater.* **2016**, *44*, 221–231. [[CrossRef](#)]
99. Tsiapalis, D.; Kearns, S.; Kelly, J.L.; Zeugolis, D.I. Growth factor and macromolecular crowding supplementation in human tenocyte culture. *Biomater. Biosyst.* **2021**, *1*, 100009. [[CrossRef](#)]
100. Huang, L.; Gu, H.; Burd, A. A reappraisal of the biological effects of hyaluronan on human dermal fibroblast. *J. Biomed. Mater. Res. A* **2009**, *90*, 1177–1185. [[CrossRef](#)]
101. Ang, X.M.; Lee, M.H.; Blocki, A.; Chen, C.; Ong, L.L.; Asada, H.H.; Sheppard, A.; Raghunath, M. Macromolecular crowding amplifies adipogenesis of human bone marrow-derived mesenchymal stem cells by enhancing the pro-adipogenic microenvironment. *Tissue Eng. Part A* **2014**, *20*, 966–981. [[CrossRef](#)] [[PubMed](#)]
102. Lee, M.H.; Goralczyk, A.G.; Kriszt, R.; Ang, X.M.; Badowski, C.; Li, Y.; Summers, S.A.; Toh, S.A.; Yassin, M.S.; Shabbir, A.; et al. ECM microenvironment unlocks brown adipogenic potential of adult human bone marrow-derived MSCs. *Sci. Rep.* **2016**, *6*, 21173. [[CrossRef](#)]
103. Obrink, B. A study of the interactions between monomeric tropocollagen and glycosaminoglycans. *Eur. J. Biochem.* **1973**, *33*, 387–400. [[CrossRef](#)]
104. Obrink, B. The influence of glycosaminoglycans on the formation of fibers from monomeric tropocollagen in vitro. *Eur. J. Biochem.* **1973**, *34*, 129–137. [[CrossRef](#)] [[PubMed](#)]